J Mater Sci (2011) 46:357–364
DOI 10.1007/s10853-010-4841-5

Formation of intermetallic phases in diffusion-welded joints of aluminium and magnesium alloys

D. Dietrich · D. Nickel · M. Krause · T. Lampke · M. P. Coleman · V. Randle

Received: 7 June 2010 / Accepted: 14 August 2010 / Published online: 31 August 2010

Abstract Basic research has been done on diffusion-welded joints with the overall aim of an adjusted interface design. The phase formation of aluminium alloy/magnesium alloy bonds has been revealed by X-ray diffraction, energy-dispersive spectroscopy and electron back-scatter diffraction. The presence of $Al_{12}Mg_{17}$ and Al_3Mg_2 phases in a bi-layer has been confirmed. The distribution and microstructure of the formed intermetallics and the arrangement of the precipitates originating from the alloys have been determined. Precipitates originating from the alloys agglomerate in the bi-layered welding zone. Their arrangement in combination with the grain boundary evolution of the intermetallics and the change of the aluminium base solid solution in the interface region has a significant influence on the mechanical properties of the joint.

Introduction

Due to the constant shortage of resources, weight reduction by substitution of Mg and Al alloys for steels is a predominant issue for the development of innovative products. Appropriate joining technologies are necessary for innovative lightweight construction materials for safety relevant applications. Thermal cracking, oxide inclusions and formation of brittle intermetallics frequently occur in conventional fusion welding techniques. The solid state nature of the friction stir welding (FSW) technology makes this process well suited for producing dissimilar Al to Mg alloy weld joints [1, 2]. Another research activity concerns the Al/Mg-co-extrusion process. The interface which is developed during this solid state process is of special interest. The main task is the examination of microstructure in context with mechanical and thermal properties of the semi-finished product. Based on the experimental analysis, the future aim is the development, implementation and application of suitable damage models to allow the simulation of the interface behaviour in view of the adhesive strength [3]. Generating Al/Mg composites by extrusion linking is widely used. The possibilities to test and evaluate relevant parameters of the bonding process are demonstrated, e.g. in [4] where the formation of a biphasic interface (Al_3Mg_2 and $Al_{12}Mg_{17}$) has been shown.

Diffusion-welding is another solid state process which has been chosen for detailed studies concerning the formation of intermetallic phases in the compound interface. Based upon the diffusion of atoms across the interface at a temperature below the eutectic temperature it is accomplished without the need for fused phases in a liquid state interface. The relevance of alloying elements, particularly silicon, is reported which has potential to control the diffusion process [5].

The studies in this paper are focused on the formation and characterisation of the bi-layered intermetallic phases in the compound interface as well as the distribution of dispersoid intermetallic particles originating from the chemical compositions of the commercially available alloys EN AW-6082 and Mg-AZ31. The identification of correlations between joining parameters (temperature, time), microstructure (phases, grain size, dimension of the

D. Dietrich (✉) · D. Nickel · M. Krause · T. Lampke
Institute of Material Science and Engineering, Chemnitz University of Technology, 09107 Chemnitz, Germany
e-mail: dagmar.dietrich@mb.tu-chemnitz.de

M. P. Coleman · V. Randle
School of Engineering, Swansea University, Swansea SA2 8PP, UK
e-mail: v.randle@swansea.ac.uk

diffusion zone, distribution of precipitates) and mechanical properties (hardness, strength) are examined in order to contribute to an adjusted interface design for Al/Mg composites.

Experiments

EN AW-6082 aluminium and AZ31 magnesium alloys (Table 1) were subjected to a diffusion-welding process under normal atmospheric conditions. Prior to joining, the bars have been ground to a surface roughness R_z of 0.2 μm (EN AW-6082), respectively, 0.3 μm (AZ31) and rinsed with ethanol. Typically, the bonding temperature was held below eutectic temperature (430 °C) and the bonding time was varied between 15 and 120 min. The bonding pressure, typically starting at 11 MPa, was lowered down to 3 MPa during the joining time thus preventing plastic deformation of the base materials. For comparison, welds were prepared at 5 K above the eutectic temperature.

For SEM investigations, cross-sections were prepared with a final oxide polish (OP-S). Phase identification was done by XRD (X-ray diffractometer Siemens D 5000). For phase localisation, the samples were studied by EBSD using two different systems. The first one was a scanning electron microscope, SEM PHILIPS XL30, equipped with an EBSD system HKL Technology Channel 5, Twist + Tango, operated at 20 kV and spot size 4. The second one was a field emission scanning electron microscope, Zeiss NEON 40EsB, equipped with an EBSD system EDAX TSL OIM 5.2 operated at 10 kV in the high current mode with a 30 μm aperture. The step size was 500 and 300 nm. The latter was chosen to obtain more detailed information. The elemental composition was recorded by EDS data collection (EDAX), either in parallel or simultaneously with the EBSD data acquisition. After EBSD data acquisition, a slight cleanup procedure was established comprising neighbour confidence index (CI) correlation, grain CI standardization with a minimum confidence index of 0.1 and grain dilatation with few iteration steps. Microindentation hardness testing (HM2000 XYm, HELMUT FISCHER GmbH) was used to determine the distribution of the Martens hardness as well as further parameters like the elastic indentation modulus across the weld. Vickers hardness has been re-evaluated from this measurement according to ISO 14577-1:2002, appendix F.

Results and discussion

Microstructure

According to the phase diagram of the aluminium–magnesium system [6] and under the condition of diffusion control, two sequential layers of intermetallic phases are expected to be formed [7] during the diffusion-welding: Al_3Mg_2 and $Al_{12}Mg_{17}$. The thickness of the phases between the diffusion-welded alloys has been calculated based on Fick′s first law. The thickness of the intermetallic phases according to the diffusion constants and activation energies published in [8] has been calculated (Table 2) and compared to the experimental values. Figure 1 shows the time-dependent phase thickness growth at 703 K. The experimental values are in satisfactory agreement with the calculation (solid lines).

Phase thickness was determined by optical and scanning electron microscopy on cross-sections. Imaging by back-scattered electrons provides a satisfactory material contrast due to the different mean atomic numbers (Fig. 2a). Occasionally, orientation contrast has been observed for the intermetallics which provide some information about grain growth (Fig. 2b). Typically, the two phases in the joint can be distinguished clearly and a multitude of precipitates is observed which originate from the aluminium and magnesium alloying. Welding results in fused phases if operated some degrees above the eutectic temperature. As a result, the intermetallic zones are reduced in width and contain more accumulated precipitates since fused intermetallics partially flow out of the joint due to the bonding pressure. The higher the joining temperature the higher is the concentration of the alloy-bearing precipitates in the $Al_{12}Mg_{17}$ phase (Fig. 3a).

The Al_3Mg_2 and $Al_{12}Mg_{17}$ phases have been identified by XRD. The integral composition of the regions of interest derived from EDS analysis confirms this finding (Table 3). A typical concentration profile of the elements aluminium, magnesium and silicon across the interface is shown in Fig. 4. This line scan refers to the sample shown in Fig. 2a. The silicon distribution marks a layer with accumulated precipitates at the Al_3Mg_2 aluminium alloy interface. The striking rise of the silicon concentration in this region is assumed as a result of the aluminium diffusion into the intermetallic phases leaving the $MgSi_2$ precipitates behind. Hence, an accumulation takes place. Moreover an

Table 1 Composition of EN AW-6082 and AZ 31 [22, 23]

	Al	Si	Mn	Zn	Cr, Fe, Cu, Ti	Mg
EN AW-6082 T4	Balance	0.7–1.3	0.40–1.0	0.20	<0.50	0.6–1.2
AZ 31 B	2.5–3.5	<0.1	0.2–0.6	0.7–1.3	–	Balance

Table 2 Diffusion constant and activation energy of Al_3Mg_2 and $Al_{12}Mg_{17}$ [8]

	Al_3Mg_2	$Al_{12}Mg_{17}$
D_0 ($m^2\ s^{-1}$)	3.5×10^{-8}	0.1
Q (kJ mol^{-1})	69 ± 4	165 ± 6

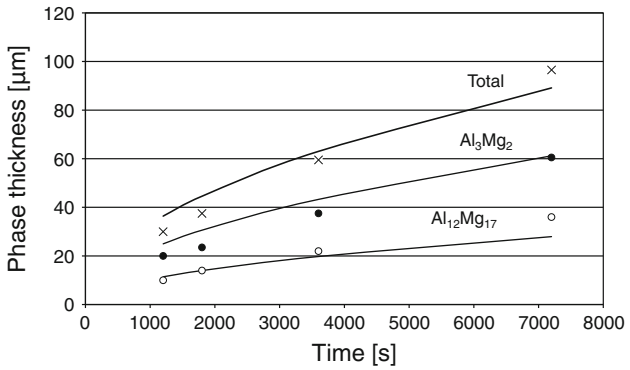

Fig. 1 Time-dependent phase thickness growth at 703 K

enhancement of the magnesium content in the aluminium base solid solution is recognised in the adjacent alloy region. The solubility of magnesium in aluminium at the used diffusion-welding temperature is about 15 at.%. Under non-equilibrium conditions, the amount of dissolved magnesium ranges from 3 to 6 at.% at room temperature in alloys with lower magnesium content [6, 9]. This has to be noticed due to the influence on mechanical properties and will be discussed later.

By use of EBSD we gained insight into the formation of the intermetallics. Typically, the Kikuchi pattern quality maps (Figs. 5a, 7a) show two layers of grains between the alloys (compare Fig. 3a and 2a). Both layers were indexed automatically as $Al_{12}Mg_{17}$ using the HKL EBSD system (Fig. 5b). Use of the TSL system resulted in correct automatic indexing of the $Al_{12}Mg_{17}$ phase adjacent to the magnesium alloy. Without operating the ChI scan (chemical indexing assisted by EDS analysis) the intermetallic layer adjacent to the aluminium alloy was automatically indexed as magnesium which is apparently incorrect; Al_3Mg_2 is

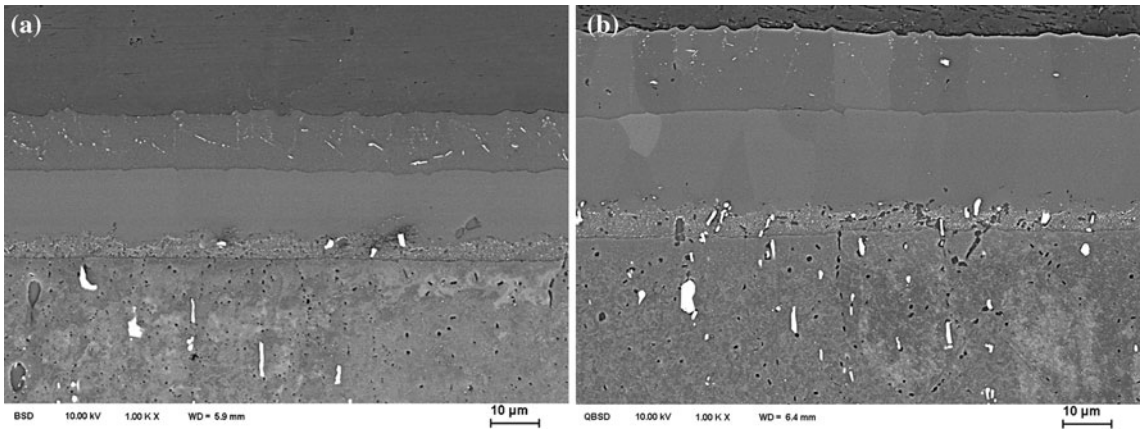

Fig. 2 **a** Al/Mg joint (*upper part* AZ 31, *lower part* EN AW-6082), diffusion-welding at 703 °C for 1200 s. **b** Al/Mg joint (*upper part* AZ 31, *lower part* EN AW-6082), diffusion-welding at 703 °C for 1800 s

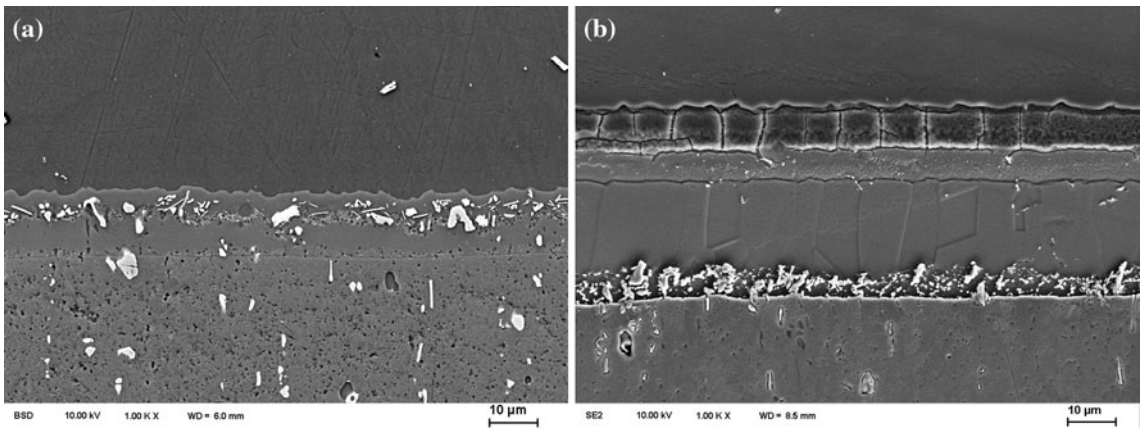

Fig. 3 **a** Al/Mg joint (*upper part* AZ 31, *lower part* EN AW-6082), welding above the eutectic temperature at 708 K. **b** Al/Mg joint after etching in 10% HF etching (same region as in Fig. 2b)

expected and confirmed by XRD measurements. The dispersoid precipitates are known from alloy specifications. Due to the used step size (500 nm) it appears hardly possible to detect reliably such submicron-scaled precipitates (Fig. 5b). However, similar examinations have been published [10–12] revealing the presence of precipitates after reheating of aluminium alloys in the semi-solid range.

Table 3 Integral composition (at.%) of the regions of interest

Region of interest	Al	Si	Mn	Zn	Mg
Magnesium alloy	6.8	0.05	0.18	0.3	92.6
$Al_{12}Mg_{17}$	44.2	0.05	0.15	0.3	55.3
Al_3Mg_2	58.9	0.09	0.08	0.2	40.8
Al_3Mg_2 with agglomerated precipitates	59.7	3.2	1.0	0.3	35.8
Aluminium alloy	95.4	0.4	0.25	0.07	3.9

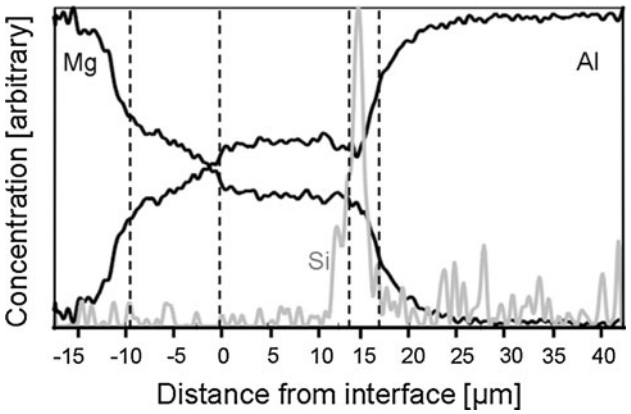

Fig. 4 EDS line scan of the Mg, Al and Si distribution across the following five phase regions: magnesium alloy, $Al_{12}Mg_{17}$, Al_3Mg_2, Al_3Mg_2 with accumulated precipitates, aluminium alloy

The Kikuchi patterns have been simulated by means of both the HKL Twist and the TSL phase software using the lattice parameters according to Table 4 and the Wyckoff positions published in [13, 14]. The structure of $Mg_{17}Al_{12}$ is of moderate complexity with a body centred cubic structure of Laves phase type fragments—an ordered binary variant of the α-Mn structure type comprising 58 atoms. The giant unit cell of the face centred cubic Al_3Mg_2 with a nearly threefold lattice constant comprises 1,168 atoms instead of 1,832 atoms rather expected from the multiplicity of the Wyckoff positions. Recently, the crystal parameters of the so-called 'Samson' phase have been confirmed and visualised in detail. Many of the partially occupied sites are due to the different orientations of the structural fragments generating split positions [15, 16]. On this basis it is possible to differentiate the Kikuchi patterns of the $Mg_{17}Al_{12}$ and the Al_3Mg_2 phase (Fig. 6). However, there are a number of metastable Al–Mg phases with cubic symmetry in the vicinity of the stability range of the Samson phase. Moreover, for the composition $Mg_{38.5}Al_{61.5}$, the cubic phase with a lattice parameter $a = 2.8242$ nm undergoes at 214 °C a first-order phase transition to a rhombohedral phase Al_3Mg_2 with $a = 1.9968$ nm and $c = 4.89114$ nm.

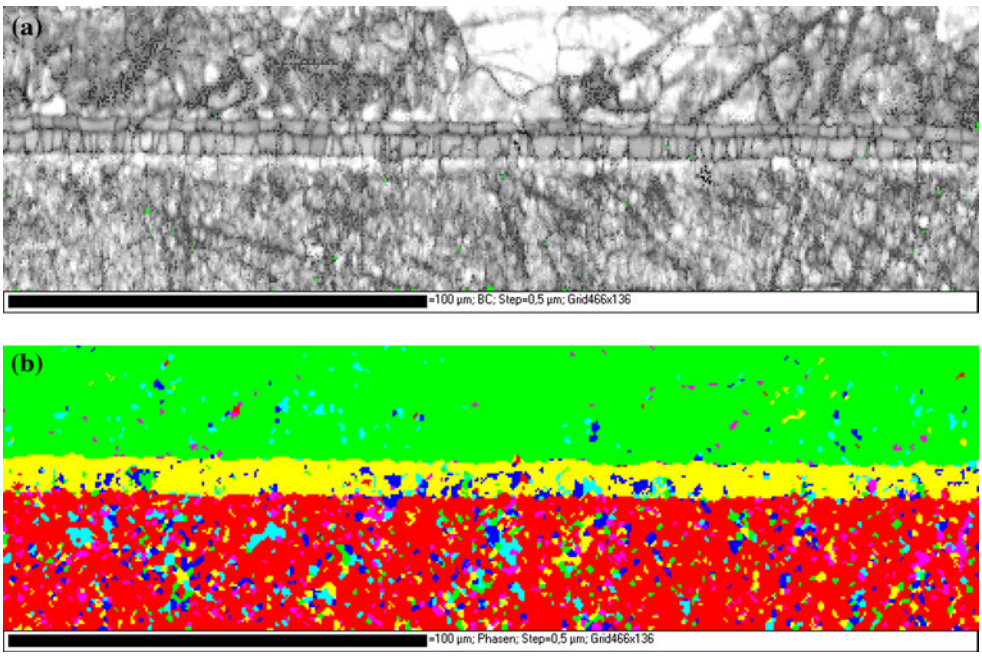

Fig. 5 **a** Kikuchi pattern quality map from the same region as Fig. 3a. **b** EBSD phase map from the same region as Fig. 3a. Colour legend: *red/dark gray* Al, *green/gray* Mg, *yellow/bright gray* $Al_{12}Mg_{17}$ (Color figure online)

Table 4 Lattice parameters (nm) of the alloys, intermetallics and precipitates

Unit cell	Al Cubic	Al(Mg) Cubic	Mg Hexagonal	Al_3Mg_2 Cubic	$Al_{12}Mg_{17}$ Cubic	$MgSi_2$ Cubic	$Al_{12}Mn_3Si$ Hexagonal	Al_6Mn Orthorhombic
a	0.405	0.409	0.320	2.824	1.054	0.635	0.751	0.755
b	0.405	0.409	0.320	2.824	1.054	0.635	0.751	0.650
c	0.405	0.409	0.519	2.824	1.054	0.635	0.774	0.887

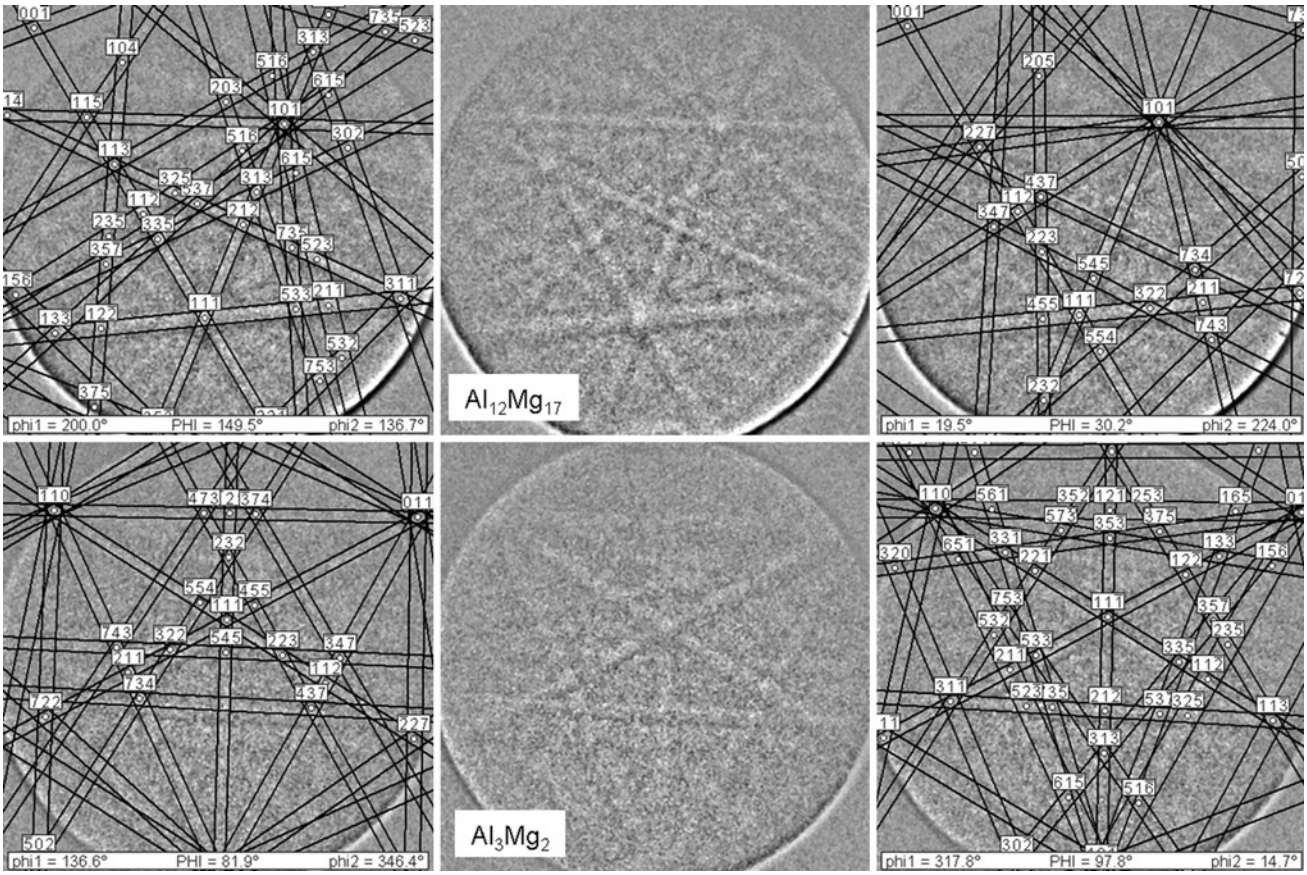

Fig. 6 Kikuchi pattern of the Laves phase $Al_{12}Mg_{17}$ (*upper row*) and the Samson phase Al_3Mg_2 (*lower row*) with correct indexing (*left column*) and incorrect indexing by the other phase (*right column*)

Except for Al_3Mg_2, automatic EBSD phase discrimination proved satisfactory considering the lattice distortions due to the mechanical preparation. In addition, the image quality of the Kikuchi patterns of the complex intermetallics is even lower compared to the fairly low image quality of the Al and Mg patterns. Hence, incorrect automatic indexing frequently occurs in the Al_3Mg_2 region as a consequence of the experimental difficulties as well as the phase structure and possible polymorphy. As a consequence the pattern fit is strikingly low. A good and time-saving solution seems to be the use of the EDS information (ChI scan). We proved this with a lower step size (300 nm) on an intermetallic bi-layer of 30 μm thickness (Fig. 2a). Equally, the Kikuchi pattern quality map of this sample shows two layers of grains between the alloys (Fig. 7a). It should be interposed here that the bright appearance of a strip of the aluminium alloy at the interface indicates remarkably higher Kikuchi pattern quality (Figs. 5a, 7a). This is the region of the aluminium solid solution with an enhanced Mg concentration. The chemical information by EDS provides the different aluminium–magnesium ratios and serves as proper phase discrimination (Fig. 7b). Moreover, by means of silicon distribution and manganese distribution the indexing of $MgSi_2$ precipitates (blue) and of $Al_{12}Mn_3Si$ precipitates (magenta) has been established. The resolution is fairly coarse compared to the better resolution of the dispersoid intermetallics distribution derived by EBSD phase discrimination. The spatial resolution of

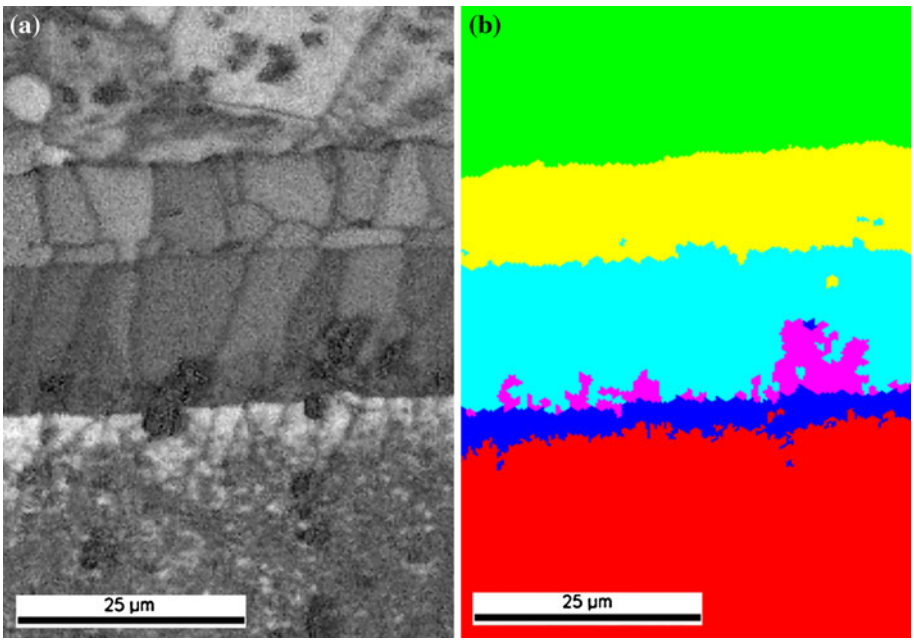

Fig. 7 Kikuchi pattern quality map (**a**) from the same region as Fig. 2a. **b** EBSD phase map from the same region as Fig. 2a. Colour legend *red/dark gray* Al, *green/gray* Mg, *yellow/bright gray* $Al_{12}Mg_{17}$, *turquoise/ middle gray* Al_3Mg_2, *blue/black* Mg_2Si (Color figure online)

EDS chemical analysis is limited by the micron-size interaction volume of elastically scattered electrons in contrast to the rather high EBSD resolution in the range of 20 nm.

Preferential chemical etching by Flick's reagent (aqueous solution of 10% HF) has been used as a complementary method to confirm grain boundaries in the Al_3Mg_2 and $Al_{12}Mg_{17}$ phases (Figs. 5a, 7a) and to show them by optical and SEM imaging (Fig. 3b). Moreover, the intermetallic phase $Al_{12}Mg_{17}$ shows two distinct layers with different etching rates and different surface appearance. Such behaviour is usually caused by a different chemical constitution. A difference in dissolved alloying elements can be assumed, but not confirmed due to the detection limit of EDS.

The base materials are characterised by fibre textures evolved from the manufacturing process by extrusion. The aluminium alloy has a texture consisting of ⟨111⟩ and ⟨100⟩ fibres along with the extrusion axes which is typical for this material [17]. In the magnesium alloy region, a relatively low number of grains contributes to the EBSD data record, but suggests the magnesium extrusion texture consisting of ⟨1010⟩ and ⟨1120⟩ fibres [17]. The cubic $Al_{12}Mg_{17}$ phase shows a weak ⟨111⟩ fibre texture in the welding plane with the axis perpendicular to the fibre axis of the extruded aluminium. This suggests a crystal formation and orientation influenced by the temperature gradient from the surface to the centre of the welded rod (Fig. 8).

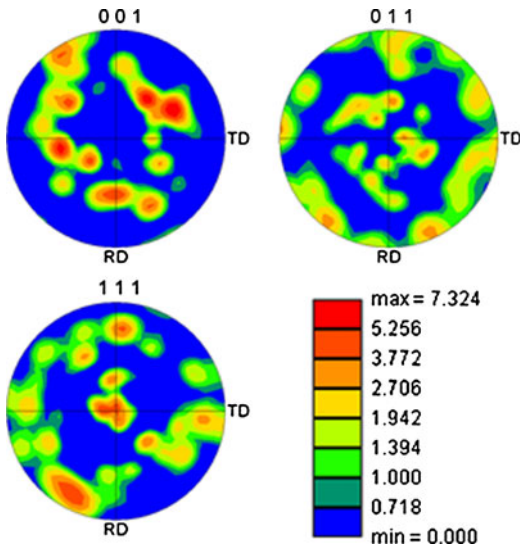

Fig. 8 Texture of $Al_{12}Mg_{17}$ in the weld plane, displayed on a {111} pole figure

Mechanical properties

Micro-indentation hardness testing was used to study the hardness and elastic modulus characteristics of the welding zone. A typical example is represented in Fig. 9. Vickers hardness has been re-evaluated from the Martens hardness evaluation. The Vickers hardness characteristic (experimental data marked by rhombohedra in Fig. 9) starts with a typical value of 75 HV 0.01 in the magnesium region [18] and rises noticeably in the region of the intermetallic phases, followed by a decrease to 70 HV 0.01 in the aluminium region as expected for the T4 temper of EN AW-6082. In the interface region between the intermetallic Al_3Mg_2 and aluminium alloy the hardness exceeds the values in both intermetallic regions which was not expected. Typically, the heat-affected zone (HAZ) of aluminium–aluminium welds (even formed by FSW [19]) shows a

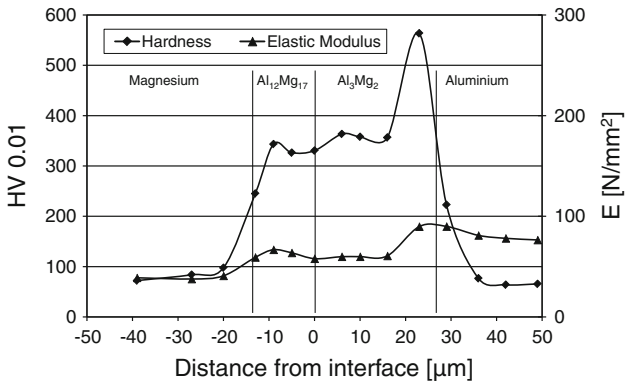

Fig. 9 Re-evaluated Vickers hardness and elastic indentation modulus characteristics of the welding zone (referring to the region in Fig. 2b)

decrease of the original hardening which can be regained by appropriate heat treatment and ageing. The remarkably enhanced hardness in this HAZ is observed for all diffusion-welded samples and has already been reflected by the Kikuchi pattern quality maps (Figs. 5a, 7a) where the pattern quality is best in this region. This is most likely due to the high hardness combined with a low plastic deformability which facilitates an artefact-free mechanical preparation of the cross-sections. Moreover enhanced magnesium concentration has been measured by EDS in this zone (compare Fig. 4). Although the joining temperature was always below the solution annealing temperature the diffusion of a higher amount of magnesium into the aluminium lattice can be assumed; even supersaturating cannot be ruled out. After diffusion-welding and quenching, the sample has been naturally aged for some months. The HAZ can be described as magnesium enhanced aluminium solid solution. The magnesium content is higher than in the proportions required for formulation of Mg_2Si, which seems to respond strongly to precipitation hardening. Besides the 6xxx series precipitates, secondary AlMg Guinier-Preston zones come into consideration, and probably earlier supposed Mg_5Al_8 precipitates [9], too. However, the ageing stages of specimens were not under investigation. Comparable studies of the kinetics of ageing and the decomposition stages of the magnesium enhanced solid solution and the existence of Guinier-Preston zones show a spinodal mode and a nucleation and growth mode of the for different temperatures [20, 21].

Also noteworthy, the $Al_{12}Mg_{17}$ hardness characteristic suggests two zones; the magnesium-adjacent and precipitate-bearing zone with rising hardness and the precipitate-free zone neighbouring Al_3Mg_2 with a uniform hardness characteristic. The non-uniformity of this phase has already been noticed by characterising the microstructure (refer to Fig. 3b). The elastic modulus characteristic (Fig. 9, experimental data marked by triangles) mirrors the values

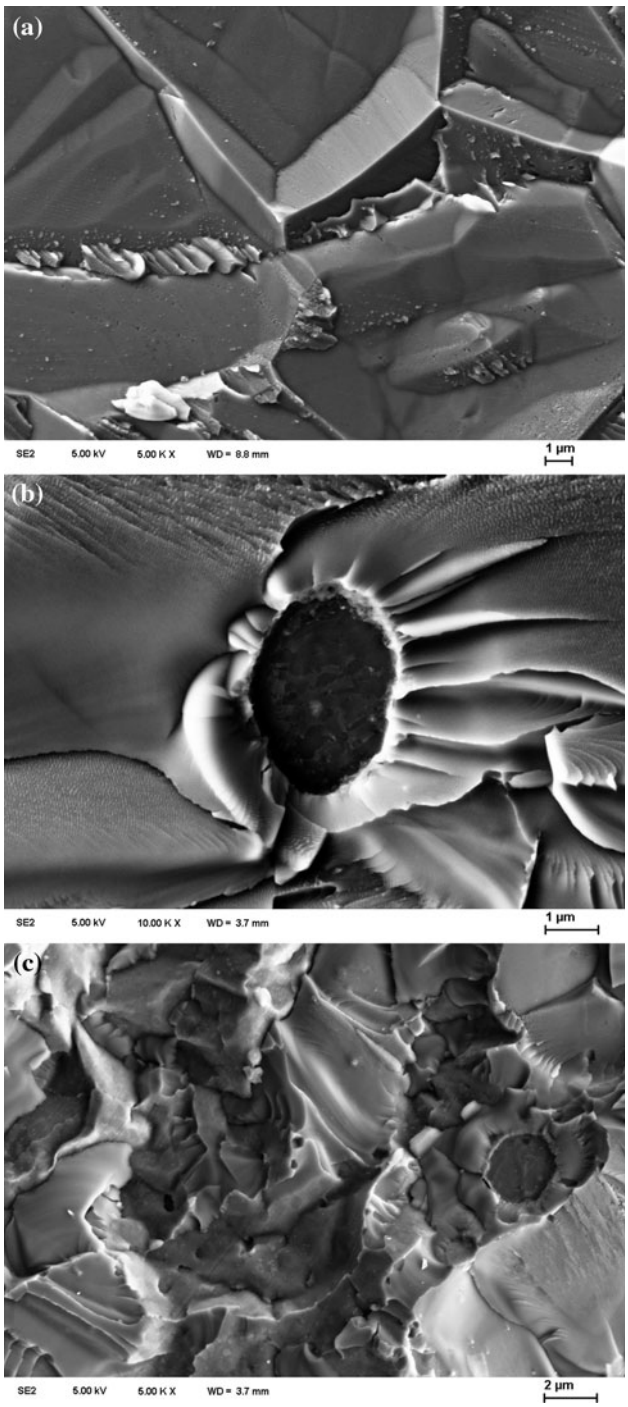

Fig. 10 Fractures in the Al_3Mg_2 phase and the adjacent aluminium HAZ, brittle-intercrystalline (**a**), brittle-transcrystalline (**b**), partly ductile (**c**)

given in [15], where the determined elastic parameters are outlined as somewhere in between those of Al and Mg. The remarkable drop of plastic deformability (65 % in the welding zone) compared to 85 or 95 % for the magnesium and aluminium alloy reflects the brittleness of the intermetallic phases Al_3Mg_2 and $Al_{12}Mg_{17}$. In the HAZ of the

aluminium alloy a plastic deformability of at least 61% has been ascertained. As a consequence of the hardness rise, the decrease of plastic deformability fractures occurs primarily in the Al_3Mg_2 phase and the adjacent aluminium HAZ. The fractures are mostly brittle; both inter-crystalline (Fig. 10a) and trans-crystalline (Fig. 10b). Micron-scale precipitates seem to act as notches. Some ductile parts can be observed in the regions where the alloy-typical precipitates have been accumulated (Fig. 10b, c). Details with the focus on mechanical properties obtained by tensile testing will be published in a further paper.

Conclusions

Basic research has been done on diffusion-welded joints with the overall aim of an adjusted interface design. The phase formation has been revealed by XRD phase identification and EBSD phase mapping. The presence of a $Al_{12}Mg_{17}/Al_3Mg_2$ bi-layer has been confirmed. The distribution and microstructure of the formed intermetallics and the arrangement of the precipitates originating from the alloys have been determined. In complement to these studies, indentation hardness testing results have been discussed. As anticipated, the ductility of the intermetallic phases is remarkably lower than the base materials. It is surprising that there is an extreme hardness rise in combination with a further drop of ductility in the aluminium alloy HAZ. As a consequence, brittle fractures occur primarily in the Al_3Mg_2 phase and the adjacent aluminium HAZ. Additionally, precipitates act as notches under load. More research has to be done in the kinetics of annealing, quenching and ageing of the diffusion-welded joints in order to contribute to an adjusted interface design for Al/Mg composites.

Acknowledgements The authors greatly acknowledge the valuable assistance of Austin Day, Aunt Daisy Scientific Limited. The German authors thank the Deutsche Forschungsgemeinschaft (German research foundation) for the financial support in the collaborative research centre "High strength aluminium-based lightweight materials for safety components" (DFG SFB 692).

References

1. Venkateswaran P, Xu ZH, Li XD, Reynolds AP (2009) J Mater Sci 44(15):4140. doi:10.1007/s10853-009-3607-4
2. Naffakh H, Shamanian M, Ashrafizadeh F (2010) J Mater Sci 45(10):2564. doi:10.1007/s10853-010-4227-8
3. Kittner K, Awiszus B (2010) Key Eng Mater 424:129
4. Neugebauer R, Glaß R, Popp M, Nickel D (2009) Mat-wiss Werkstofftech 40(7):506
5. Wilden J, Bergmann JP, Jahn S (2006) Adv Eng Mater 8(3):212
6. (1998) ASM handbook, vol 3: alloy phase diagrams. ASM International, Metals park, OH
7. Dybkov OV, Dybkov VI (2004) J Mater Sci Lett 39:6615
8. Tanguep Njiokep EM, Salamon M, Mehrer H (2001) DDF 194–199:1581
9. Mondolfo LF (2007) Metallography of aluminium alloys. Johnson Press, Edinburgh, Scotland. ISBN 1406736724
10. Mrówka-Nowotnik G, Sieniawski J, Wierzbinska M (2007) Arch Mater Sci Eng 28(2):69
11. Liu YL, Kang SB, Kim HW (1999) Mater Lett 41(6):267
12. Vaneetveld G, Rassili A, Pierret J-C, Lecomte-Beckers J, Atkinson HV (2009) Int J Mater Form 2:777
13. Aroyo MI, Perez-Mato JM, Capillas C, Kroumova E, Ivantchev S, Madariaga G, Kirov A, Wondratschek H (2006) Z Kristallogr 221:15
14. Samson S (1965) Acta Cryst 19:401
15. Feuerbacher M, Thomas C, Makongo JPA, Hoffmann S, Carrillo-Cabrera W, Cardoso R, Grin Y, Kreiner G, Joubert J-M, Schenk T, Gastaldi J, Nguyen-Thi H, Mangelinck-Noe N, Billia B, Donnadieu P, Czyrska-Filemonowicz A, Zielinska-Lipiec A, Dubiel B, Weber T, Schaub P, Krauss G, Gramlich V, Christensen J, Lidin S, Fredrickson D, Mihalkovic M, Sikora W, Malinowski J, Brühne S, Proffen T, Assmus W, de Boissieu M, Bley F, Chemin J-L, Schreuer J, Steurer W (2007) Z Kristallogr 222:259
16. Daniel C, Fredrickson DC, Lee S, Hoffmann R (2007) Angew Chem Int Ed 46:1958
17. Vatne HE, Pedersen K, Lohne O, Jenssen G (1997) Textures Microstruct 30:81
18. Müller S, Müller K, Tao H, Reimers W (2006) Int J Mater Res/Z Melallkunde 97(10):1384
19. Lee CY, Lee WB, Kim JW, Choi DH, Yeon YM, Jung SB (2008) J Mater Sci 43:3296. doi:10.1007/s10853-008-2525-1
20. Gault C, Dauge A, Boch P (1975) Phys Stat Sol (A) 31:179
21. van Rooyen M, Sinte Maartensdijk JA, Mittemeijer EJ (1988) Metall Trans 19A:2433
22. (1995) ASM Handbook, vol 2: properties and selection: nonferrous alloys and special-purpose materials. ASM International, Metals park OH
23. Rundstangen EN (2009) AW 6082 Technisches Datenblatt. GLEICH Aluminiumwerk GmbH & Co. KG